A New Stable Algorithm to Compute Hankel Transform Using Chebyshev Wavelets

Rajesh K. Pandey[1], Vineet K. Singh[2] and Om P. Singh[3,*]

[1] *PDPM Indian Institute of Information Technology Design and Manufacturing, Jabalpur, India.*
[2] *Birla Institute of Technology and Science-Pilani, Goa Campus, Goa, India.*
[3] *Department of Applied Mathematics, Institute of Technology, Banaras Hindu University, Varanasi, India.*

Abstract. A new stable numerical method, based on Chebyshev wavelets for numerical evaluation of Hankel transform, is proposed in this paper. The Chebyshev wavelets are used as a basis to expand a part of the integrand, $rf(r)$, appearing in the Hankel transform integral. This transforms the Hankel transform integral into a Fourier-Bessel series. By truncating the series, an efficient and stable algorithm is obtained for the numerical evaluations of the Hankel transforms of order $\nu > -1$. The method is quite accurate and stable, as illustrated by given numerical examples with varying degree of random noise terms $\varepsilon\theta_i$ added to the data function $f(r)$, where θ_i is a uniform random variable with values in $[-1,1]$. Finally, an application of the proposed method is given for solving the heat equation in an infinite cylinder with a radiation condition.

AMS subject classifications: 65R10

Key words: Hankel transforms, Bessel functions, Chebyshev wavelets, random noise term.

1 Introduction

There are several integral transforms which are frequently used as a tool for solving numerous scientific problems. It is well known that the Fourier transform (FT) is used to obtain spatial spectrum of optical light [1]. Fourier optics is widely used in optical instrument design, optical propagation through lenses and in quadratics graded index mediums. Most classical optical systems like mirrors or lenses are axially symmetrical

devices. In many practical problems, data are often acquired in such a form that is desirable to perform a two-dimensional polar Fourier transform that is a Hankel transform (HT) rather than the Cartesian forms. So, we transform the Cartesian coordinates into the polar coordinates.

Let $f(x,y)$ be an input field such that it can be separated as $f(x,y) = f_1(x)f_2(y)$, where f_1 and f_2 are independent functions. Then its two-dimensional Fourier transform $\hat{f}$ is also separable as the same symmetry property is transposed through a linear FT. Hence, $\hat{f}(u,v) = \hat{f}_1(u) \cdot \hat{f}_2(v)$.

Changing to the polar coordinates and if $f(r,\theta) = f(r)$ is axially symmetrical, then in [2], it was shown that

$$\hat{f}(k,\varphi) = \frac{1}{2}\int_0^\infty d(r^2)f(r)J_0(kr) \equiv F_0(k), \tag{1.1}$$

which is also axially symmetrical in the Fourier frequency domain, where F_0 is the Hankel transform of order zero. The general Hankel transform pair with the kernel being J_ν is defined as

$$F_\nu(p) = \int_0^\infty rf(r)J_\nu(pr)dr, \tag{1.2}$$

and HT being self reciprocal, its inverse is given by

$$f(r) = \int_0^\infty pF_\nu(p)J_\nu(pr)dp, \tag{1.3}$$

where J_ν is the νth-order Bessel function of first kind.

The Hankel transform arises naturally in the discussion of problems posed in cylindrical coordinates and hence, as a result of separation of variables, involving Bessel functions. The Hankel transform is frequently used as a tool for solving numerous scientific problems. It is widely used in several fields like, elasticity [4], optics [5,6], fluid mechanics [7], seismology [8], astronomy and image processing [9–16]. The Hankel transform becomes very useful in analysis of wave fields where it is used in mathematical handling of radiation, diffraction, and field projection. Recently, it has been utilized to study pseudo-differential operators. Singh and Pandey [17] used HT of order ν, $\nu \in \mathbf{R}$ to study a special class of pseudo-differential operator (PDO) $(-x^{-1}D)^\nu$, $D = d/dx$ and proved that the (PDO) is almost an inverse of HT operator h_ν in the sense that

$$h_\nu o(-x^{-1}D)^\nu(\varphi) = h_0(\varphi)$$

over certain Freshet space F, thus representing the PDO as a Fourier-Bessel series. Further, in 1995, Singh [18], using the HT representation of the PDO, proved that $e^{-\alpha x^2}$, $\text{Re}\,\alpha > 0$ are the eigenfunctions and $e^{-x^2/2}$ is a fixed point of $(-x^{-1}D)^\nu$, $\nu \in \mathbf{C}$.

Several papers have been written to the evaluation of the Hankel transform in general and the zeroth order in particular. Analytical evaluations of (1.2) and (1.3) are rare and their numerical computations are difficult because of the oscillatory behavior of the Bessel function and the infinite length of the interval. Since seminal work by Siegman [19] in 1977, a number of algorithms for the numerical evaluation of the Hankel transform have been published for both zero-order [5,6,9–12,20–24] and high-order [25–33] Hankel transform. Unfortunately, the efficiency of a method for computing Hankel transform is highly dependent on the function to be transformed, and thus it is difficult to choose the optimal algorithm for given function. In [21], the authors used Filon quadrature Philosophy to evaluate zero-order Hankel transform. They separated the integrand into the product of (assumed) slowly varying component and a rapidly oscillating one (in this case, former is $rf(r)$ and the later is $J_\nu(pr)$). This methods works quite well for computing $F_0(p)$, for $p \geq 1$, but the calculation of inverse Hankel transform is more difficult, as $F_0(p)$ is no longer a smooth function but a rapidly oscillating one. Moreover, the error is appreciable between $0 < p < 1$. In 1998, Yu et al. [23] gave another method to compute zero-order quasi discrete HT by approximating the input function by a Fourier-Bessel series over a finite integration interval. It lead to a symmetric transformation matrix for the HT and the IHT that satisfies the discrete form of the Parseval theorem.

Later in 2004, Guizar-Sicairos et al. [34] obtained a powerful scheme to calculate the HT of integer order $\nu \geq 0$ by extending the zero-order HT algorithm of Yu [23] to higher orders. Their algorithm is based on the orthogonality properties of Bessel functions. Postnikov [32], proposed, for the first time, a novel and powerful method for computing zero and first order HT by using Haar wavelets. Refining the idea of Postnikov [32], we [35,36] obtained two more algorithms for numerical evaluation of HT of order $\nu > 1$ using linear Legendre multi-wavelets and rationalized Haar wavelets which were shown to be superior to the other mentioned algorithms.

The data function $f(r)$ when measured experimentally may contain some noise terms affecting the accuracy of the algorithms for computing the HT. Thus, it is desirable to have algorithms stable under small random perturbation in the data function.

The purpose of this communication is to present a stable algorithm that is quite accurate and fast for numerical evaluation of the HT using Chebyshev wavelets. Test functions with known analytic HT are used with random noise term $\varepsilon\theta_i$ added to the data function $rf(r)$, where θ_i is a uniform random variable with values in $[-1,1]$, to illustrate the stability and efficiency of the proposed algorithm. As an application of the theory developed, we solve the heat flow problem in an infinite cylinder with radiation condition.

2   The Chebyshev wavelets

Wavelets are a class of function constructed from dilation and translation of a single function called the mother wavelet. When the dilation and translation parameters a and b

vary continuously, the following family of continuous wavelets are obtained

$$\psi_{ab}(t) = |a|^{-1/2}\psi\left(\frac{t-b}{a}\right), \qquad a,b \in \mathbf{R}, \quad a \neq 0.$$

When the parameters a and b are restricted to discrete values as $a = 2^{-k}$, $b = n2^{-k}$, then, we have the following family of discrete wavelets

$$\psi_{kn}(t) = 2^{k/2}\psi(2^k t - n), \qquad k,n \in Z,$$

where the function ψ, the mother wavelet, satisfies $\int_R \psi(t)dt = 0$.

We are interested in the case where ψ_{kn} constitutes an orthonormal basis of $L^2(\mathbf{R})$. A systematic way to do this is by means of multiresolution analysis (MRA).

In 1910, Haar [37] constructed the first orthonormal basis of compactly supported wavelets for $L^2(\mathbf{R})$. It has the form $\{2^{j/2}\psi(2^j t - k) : j,k \in Z\}$ where the fundamental wavelet ψ is constructed as follows: Construct a compactly supported scaling function φ by the two-scale scaling relation $\varphi(t) = \varphi(2t) + \varphi(2t-1)$ together with the normalization constraint $\int \varphi(t)dt = 1$. A solution of this recursion that represents φ in $L^2(\mathbf{R})$ is $\chi_{[0,1)}$. Then $\psi(t) = \varphi(2t) - \varphi(2t-1)$. The Haar wavelets are piecewise continuous and have discontinuities at certain dyadic rational numbers.

In seminal papers; Daubechies [38,39], constructed the first orthonormal basis of continuous compactly supported wavelets for $L^2(\mathbf{R})$. They have led to a significant literature and development, both in theoretical and applied arenas.

Later in 1989, Mallet [40] studied the properties of multiresolution approximation and proved that it is characterized by a 2π-periodic function. From any MRA, one can derive a function $\psi(t)$ called a wavelet such that $\{2^{j/2}\psi(2^j t - k) : j,k \in Z\}$ is an orthonormal basis of $L^2(\mathbf{R})$. The MRA showed the full computational power that this new basis for $L^2(\mathbf{R})$ possessed. In the same year, Mallet [41] applied MRA for analyzing the information content of the images.

Note that a system $\{\varphi_k : k \in Z\}$ is called a Riesz basis if it is obtained from an orthonormal basis by means of a bounded invertible operator [42].

Definition 2.1. *The increasing sequence* $\{V_k\}_{k \in Z}$ *of closed subspaces of* $L^2(\mathbf{R})$ *with scaling function* $\varphi \in V_0$ *is called MRA if*

  (i). $\bigcup_{\mathbf{k}} V_k$ *is dense in* $L^2(\mathbf{R})$ *and* $\bigcap_{\mathbf{k}} V_k = \{0\}$,

 (ii). $f(t) \in V_k$ *iff* $f(2^{-k}t) \in V_0$,

(iii). $\{\varphi(t-n)\}_{n \in Z}$ *is a Riesz basis for* V_0.

Note that (iii) implies that the sequence $\{2^{k/2}\varphi(2^k t - n)\}_{k,n \in Z}$ is an orthonormal basis for V_k.

Let $\psi(t)$ be the mother wavelet, the $\psi(t) = \sum_{n \in Z} a_n \varphi(2t - n)$ and $\{2^{k/2}\varphi(2^k t - n)\}_{k,n \in Z}$ forms an orthonormal basis for $L^2(\mathbf{R})$ under suitable conditions [38].

For $k=1,2,3,\cdots$ and $n=1,2,3,\cdots,2^{k-1}$, the Chebyshev wavelets $\psi_{nm}(t)$ are defined as [43]

$$\psi_{nm}(t) = \begin{cases} 2^{k/2}\widetilde{T}_m(2^k t - 2n + 1), & \text{for } \dfrac{n-1}{2^{k-1}} \leq t < \dfrac{n}{2^{k-1}}, \\ 0, & \text{otherwise,} \end{cases} \tag{2.1}$$

where

$$\widetilde{T}_m(t) = \begin{cases} \dfrac{1}{\sqrt{\pi}}, & m=0, \\ \sqrt{\dfrac{2}{\pi}}T_m(t), & m>0, \end{cases} \tag{2.2}$$

and t is the time. The well known Chebyshev polynomials $T_m(t)$ of the first kind and of degree m are orthogonal with respect to the weight function $w(t) = 1/\sqrt{1-t^2}$. They are defined on [-1,1] by the following recurrence relation:

$$T_0(t) = 1, \quad T_1(t) = t \quad \text{and} \quad T_{m+1}(t) = 2tT_m(t) - T_{m-1}(t), \quad m=1,2,3,\cdots.$$

Note that in dealing with Chebyshev wavelets the weight function $w(t)$ have to be dilated and translated as

$$w_n(t) = w(2^k t - 2n + 1),$$

to get orthogonal wavelets forming an orthonormal basis for $L^2_w[0,1]$.

3 Outline of algorithm

The function $f(r)$ representing physical fields are either zero or have an infinitely long decaying tail outside a disk of finite radius R. Hence, in most practical applications either the signal $f(r)$ has a compact support or for a given ε there exists a $R>0$ such that

$$\left| \int_R^\infty rf(r)J_v(pr)dr \right| < \varepsilon,$$

which is the case if $f(r) = \mathcal{O}(r^\eta)$, as $r \to \infty$, where $\eta < -3/2$. Therefore, in either case,

$$\hat{F}_v(p) = \int_0^R rf(r)J_v(pr)dr = \int_0^1 rf(r)J_v(pr)dr \quad \text{(by scaling)} \tag{3.1}$$

known as the finite Hankel transform (FHT) is a good approximation of the HT as given by (1.2). The algorithm is efficient if f decays faster than $r^{-3/2}$ outside some disk of finite radius R which includes the majority of input signals of physical interest. Writing $rf(r) = g(r)$ in equation (3.1), we get

$$\hat{F}_v(p) = \int_0^1 g(r)J_v(pr)dr. \tag{3.2}$$

We may expand $g(r)$ as follows

$$g(r) = \sum_{n=1}^{\infty} \sum_{m=0}^{\infty} c_{nm}\psi_{nm}(r), \tag{3.3}$$

where

$$c_{nm} = \langle g(r), \psi_{nm}(r) \rangle_{w_n} = \int_0^1 w_n(r)g(r)\psi_{nm}(r)dr.$$

By truncating the infinite series (3.3) at levels $n = 2^{k-1}$ and $m = M$, we obtain an approximate representation for $g(r)$ as

$$g(r) \approx \sum_{n=1}^{2^{k-1}} \sum_{m=0}^{M} c_{nm}\psi_{nm}(r) = C^T \Psi(r), \tag{3.4}$$

where the matrices C and Ψ are given by

$$C = [c_{10}, c_{11}, \cdots, c_{1M}, c_{20}, \cdots, c_{2M}, \cdots, c_{2^{k-1}0}, \cdots, c_{2^{k-1}M}]^T, \tag{3.5}$$

$$\Psi(r) = [\psi_{10}(r), \psi_{11}(r), \cdots, \psi_{20}(r), \cdots, \psi_{2M}(r), \cdots, \psi_{2^{k-1}0}(r), \cdots, \psi_{2^{k-1}M}(r)]^T. \tag{3.6}$$

Substituting (3.4) in (3.2), we get

$$\hat{F}_\nu(p) \approx C^T \int_0^1 \Psi(r)J_\nu(pr)dr. \tag{3.7}$$

Taking $M = 2$ and $k = 2$, Eq. (3.7) reduces to

$$\hat{F}_\nu(p) \approx C^T \left[\int_0^1 \psi_{10}(r)J_\nu(pr)dr, \int_0^1 \psi_{11}(r)J_\nu(pr)dr, \cdots, \int_0^1 \psi_{22}(r)J_\nu(pr)dr \right]^T, \tag{3.8}$$

where the six basis functions are given by

$$\psi_{10}(r) = \frac{2}{\sqrt{\pi}}, \quad \psi_{11}(r) = \frac{2\sqrt{2}}{\sqrt{\pi}}(4r-1), \quad \psi_{12}(r) = \frac{2\sqrt{2}}{\sqrt{\pi}}\left[2(4r-1)^2 - 1\right], \quad 0 \leqslant r < \frac{1}{2}, \tag{3.9a}$$

$$\psi_{20}(r) = \frac{2}{\sqrt{\pi}}, \quad \psi_{21}(r) = \frac{2\sqrt{2}}{\sqrt{\pi}}(4r-3), \quad \psi_{22}(r) = \frac{2\sqrt{2}}{\sqrt{\pi}}\left[2(4r-3)^2 - 1\right], \quad \frac{1}{2} \leqslant r < 1. \tag{3.9b}$$

We re-label and write Eq. (3.8) as

$$\hat{F}_\nu(p) \approx [c_0, c_1, c_2, c_3, c_4, c_5][I_\nu^0, I_\nu^1, I_\nu^2, I_\nu^3, I_\nu^4, I_\nu^5]^T, \tag{3.10}$$

where I_ν^{k}'s are $(k+1)$th place integral in Eq. (3.8) and are evaluated by using the following formulae:

$$\int_0^a J_\nu(t)\,dt = 2\lim_{N\to\infty}\sum_{n=0}^N J_{\nu+2n+1}(a), \quad \mathrm{Re}\,\nu > -1, \quad [44,\ \mathrm{p.}\ 333]$$

$$\int_0^a t^{1-\nu} J_\nu(t)\,dt = \frac{1}{2^{\nu-1}\Gamma(\nu)} - a^{1-\nu} J_{\nu-1}(a), \quad [44,\ \mathrm{p.}\ 333]$$

$$\int_0^a t^\mu J_\nu(t)\,dt = \frac{a^\mu \Gamma(\frac{\nu+\mu+1}{2})}{\Gamma(\frac{\nu-\mu+1}{2})}\lim_{N\to\infty}\sum_{n=0}^N \frac{(\nu+2n+1)\Gamma(\frac{\nu-\mu+1}{2}+n)}{\Gamma(\frac{\nu+\mu+3}{2}+n)} J_{\nu+2n+1}(a),$$

$$\mathrm{Re}(\nu+\mu+1) > 0, \quad [45,\ \mathrm{p.}\ 480]. \tag{3.11}$$

In 2004, Piessens [46] approximated the input field $g(r)$ on $[0,1]$ as

$$g(r) \approx r^\alpha \sum_{k=o}^N c_n T_k^*(r), \tag{3.12}$$

where $T_k^*(r)$ is the shifted Chebyshev polynomials of degree k and $\alpha > 0$ is a real parameter. Thus approximating the Hankel transform $\hat{F}_\nu(p)$ as,

$$\hat{F}_\nu(p) \approx \sum_{k=0}^N c_k \int_0^1 r^\alpha J_\nu(pr) T_k^*(r)\,dr$$

$$= C^T \left[\int_0^1 r^\alpha T_0^*(r) J_\nu(pr), \int_0^1 r^\alpha T_1^*(r)\,dr, \cdots, \int_0^1 r^\alpha T_N^* J_\nu(pr)\,dr\right]^T$$

$$= [c_0, c_1, c_2, \cdots, c_k]\,[M_0, M_1, M_2, \cdots, M_N]^T, \tag{3.13}$$

where

$$M_l = \int_0^1 r^\alpha T_l^*(r) J_\nu(pr)\,dr, \quad l = 0, 1, \cdots, N. \tag{3.14}$$

These modified moments M_l's (similar to I_ν^l's in Eq. (3.10)) satisfy a homogenous, linear, nine-term recurrence relation. But the forward and backward recursion are asymptotically unstable. However, the instability of forward recursion is less pronounced if $l \leqslant Rp/2$, but for $l > Rp/2$ the loss of significant figures increases and forward recursion is no longer applicable. In that case, these recurrence relations have to be solved as a boundary value problem with six initial values and two end values, making the evaluation of M_l's more difficult than that of I_ν^l's.

In our proposed method, the integrals I_ν^l $l=0,1,2,\cdots,5$ are extremely easy to evaluate. For example,

$$I_\nu^0 = \frac{2}{\sqrt{\pi}} \int\limits_0^1 J_\nu(pr)dr \approx \frac{4}{p\sqrt{\pi}} \sum_{n=0}^N J_{\nu+2n+1}(p).$$

Thus we see that these integrals I_ν^l are approximated by finite sums of different orders Bessel functions J_μ's evaluated at the particular point p. Besides the simplicity of our algorithm in computation over [46], it is also stable under the noise in the input field where as the algorithm proposed in [46] is not tested for the stability.

4 Numerical results

In this section we discuss, the implementation of our numerical method and investigate its accuracy and stability by applying it on numerical examples with known analytical HT.

In all the examples, the exact data function is denoted by $g(r)$ and the noisy data function $g^\varepsilon(r)$ is obtained by adding an ε random error to $g(r)$ such that $g^\varepsilon(r_i)=g(r_i)+\varepsilon\theta_i$, where $r_i=ih$ $i=1,2,\cdots,L$, $Lh=100$ and θ_i is a uniform random variable with values in $[-1,1]$ such that

$$\max_{0\leqslant i\leqslant L} |g^\varepsilon(r_i)-g(r_i)| \leqslant \varepsilon.$$

The following examples are solved with and without random perturbations to illustrate the efficiency and stability of our method by choosing four different values of the random error ε as $\varepsilon=0,0.001,0.002$ and 0.005 computing the error $Ej(p)=$ Approximate HT obtained from (3.10) with random error ε_i - the exact HT, $j=0,1,2,3$. The various $Ej(p)$'s are shown in Figs. 2-3, 5-6, 8-9, 11-12, 14-15 and 17-18. Note that the various graphs in the following examples are plotted by choosing the sample points as $p=0.01(0.01)P$, where $P=20$ in Figs. 1, 4, 7, 10, 13, 16 and $P=100$ in Figs. 2-3, 5-6, 8-9, 11-12, 14-15, 17-18.

We also use the discrete l^2 norm and the continuous L^2 norm in $I=[0,P]$ to measure errors as well. They are defined as:

$$\|f\|_{2,I} = \left(\frac{1}{N} \sum_{i=1}^N |f(r_i)|^2 \right)^{1/2} \tag{4.1}$$

and

$$\|f\|_2 = \left(\int\limits_0^P |f(r)|^2 dr \right)^{1/2}, \tag{4.2}$$

respectively.
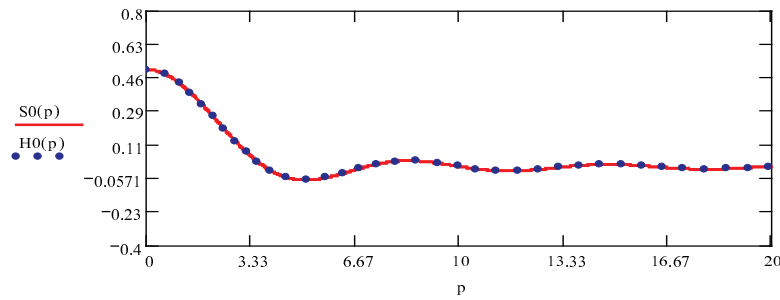
Figure 1: The exact transform, $S0(p)$ (solid line) and the approximate transform, $H0(p)$ (dotted-line) truncated at level $N=20$ and $M=2$.
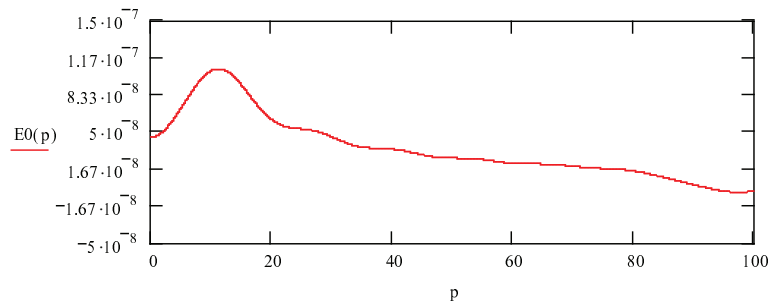
Figure 2: Error between exact transform, $S0(p)$ and approximated transform $H0(p)$ (without random noise).
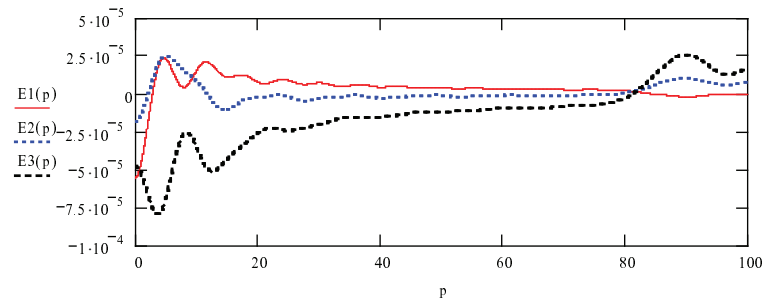
Figure 3: Errors between exact transform and approximated transform with different random perturbations.

Example 4.1 (Sombrero function). A very important, and often used function, is the Circ function that can be defined as

$$\text{Circ}(r/a) = \begin{cases} 1, & r \leqslant a, \\ 0, & r > a. \end{cases} \tag{4.3}$$

The zeroth-order HT of Circ(r/a) is the Sombrero function [47], given by $S_0(p) = a^2 \frac{J_1(ap)}{ap}$. We use Eq. (3.10) to obtain the approximation for the FHT $\hat{F}_0(p)$ of the Circ(r/a). This approximation is compared with the exact HT $S_0(p)$ and is shown in Fig. 1. Figs. 2 and 3 represent the corresponding error $E0(p)$ and $Ej(p)$, $j=1,2,3$, respectively. Note that
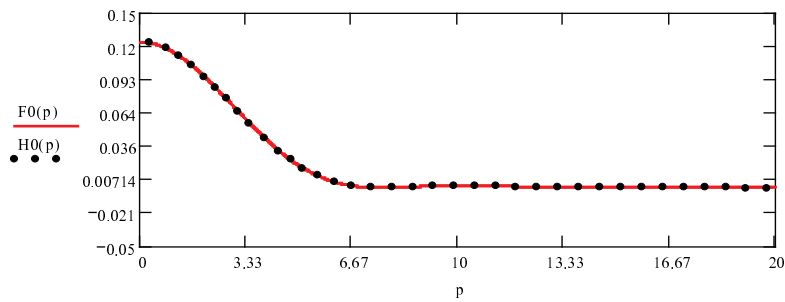
Figure 4: The exact transform, $F0(p)$ (solid line) and the approximate transform, $H0(p)$ (dotted-line) truncated at level $N=50$ and $M=2$.
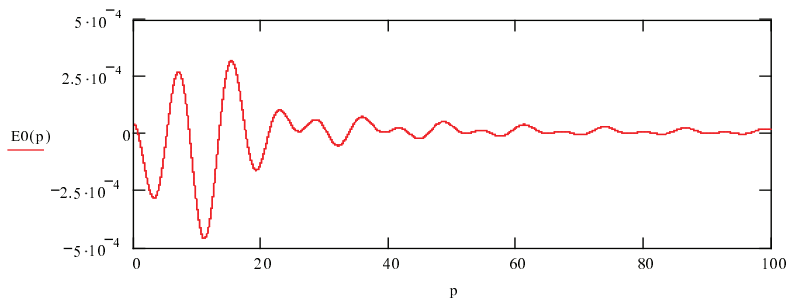
Figure 5: Error between exact transform, $F0(p)$ and approximated transform $H0(p)$ (without random noise).
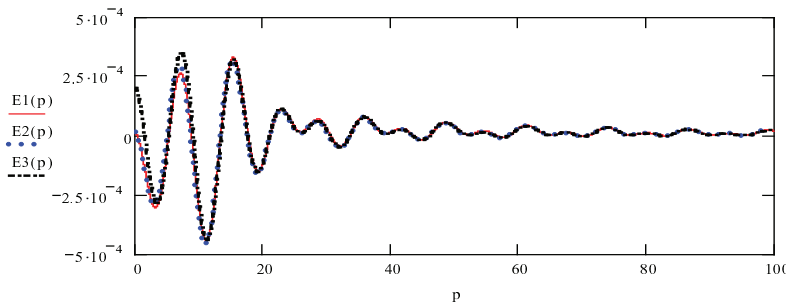
Figure 6: Errors between exact transform and approximated transform with different random perturbations.

$S_0(p)$ and $\hat{F}_0(p)$ are indicated by $S0(p)$ (solid line) and $H0(p)$ (dotted line) in Figs. 1 and 2 respectively.

Example 4.2. Let $f(r) = \frac{2}{\pi}[\arccos(r) - r(1-r^2)^{1/2}]$, $0 \leqslant r \leqslant 1$. Then,

$$F_0(p) = 2\frac{J_1^2(p/2)}{p^2}, \qquad 0 \leqslant p \leqslant \infty \quad [21]. \tag{4.4}$$

Barakat et al. [21], evaluated $F_0(p)$ numerically using Filon quadrature philosophy but the associated error is appreciable for $p > 1$; whereas our method gives almost zero error
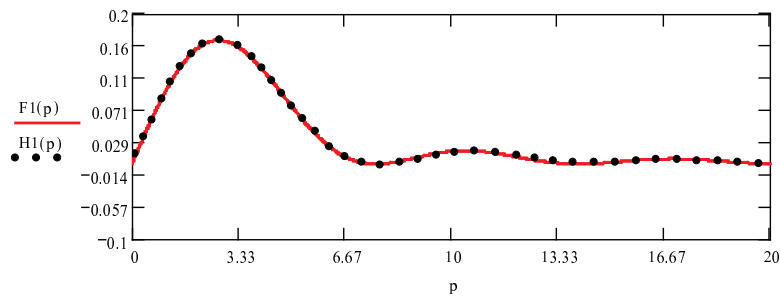
Figure 7: The exact transform, $F1(p)$ (solid line) and the approximate transform, $H1(p)$ (dotted-line) truncated at level $N=50$ and $M=2$.
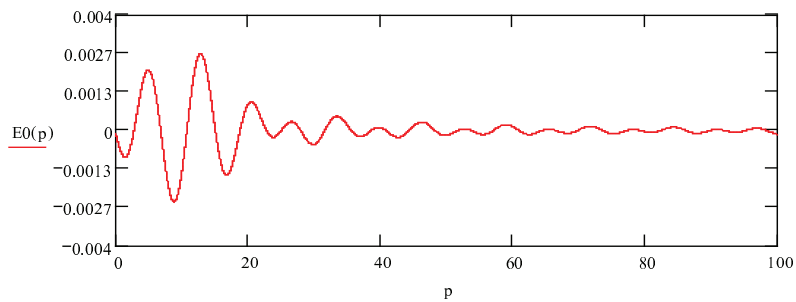
Figure 8: Error between exact transform, $F1(p)$ and approximated transform $H1(p)$ (without random noise).
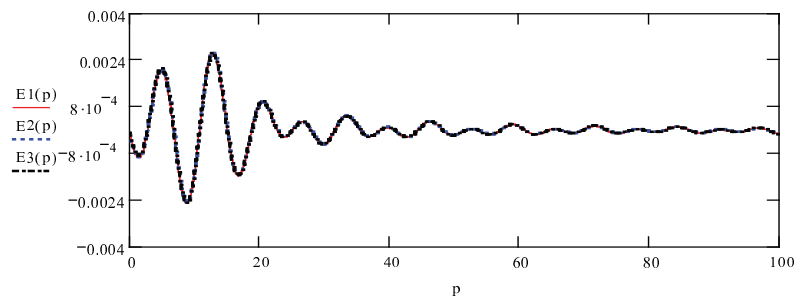
Figure 9: Errors between exact transform and approximated transform with different random perturbations.

in that range. Note that $F_0(p)$ and $\hat{F}_0(p)$ are indicated by $F0(p)$ (solid line) and $H0(p)$ (dotted line) in Fig. 4 and the corresponding error graphs $Ej(p)$ in Figs. 5 and 6.

Example 4.3. Let $f(r)=(1-r^2)^{1/2}, 0\leqslant r\leqslant1$. Then,

$$F_1(p)=\begin{cases} \pi\dfrac{J_1^2(p/2)}{2p}, & 0<p<\infty, \\ 0, & p=0. \end{cases} \tag{4.5}$$

Barakat et al. [22], evaluated $F_1(p)$ numerically using Filon quadrature philosophy but again the associated error is appreciable for $p<1$; whereas our method give almost zero
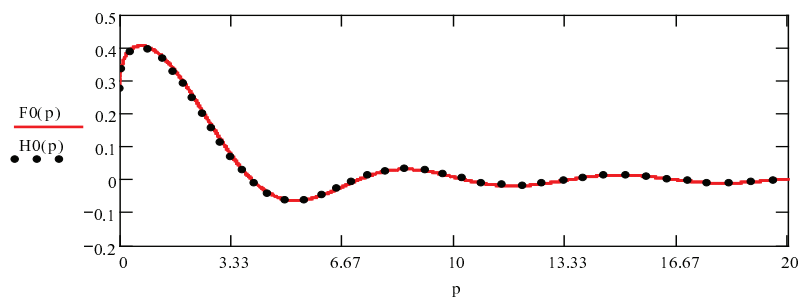
Figure 10: The exact transform, $F0(p)$ (solid line) and the approximate transform, $H0(p)$ (dotted-line) truncated at level $N=50$ and $M=2$ ($\nu=1/10$).
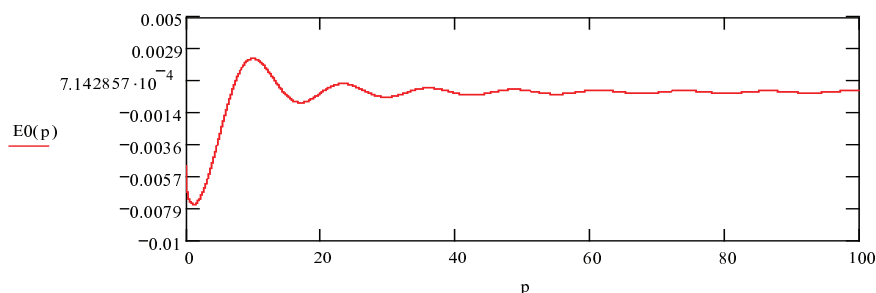
Figure 11: Error between exact transform, $F0(p)$ and approximated transform $H0(p)$ (without random noise) ($\nu=1/10$).
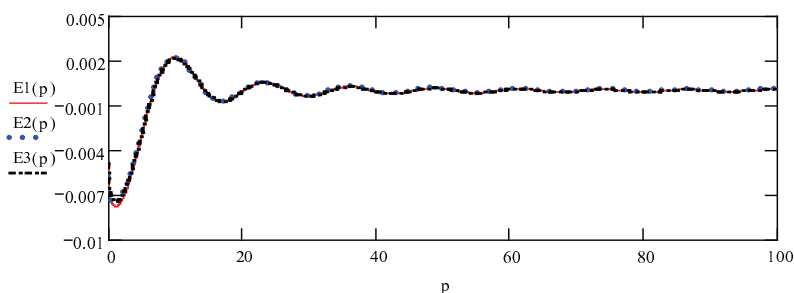
Figure 12: Errors between exact transform and approximated transform with different random perturbations ($\nu=1/10$).

error in that range. The comparison of the approximation $H1(p)$ (dotted line) with the exact HT $F1(p)$ (solid line) is shown in Fig. 7 and the corresponding error graphs $Ej(p)$ in Figs. 8 and 9.

Example 4.4. In this example, we choose as a test function the generalized version of the top-hat function, given as $f(r)=r^{\nu}[H(r)-H(r-a)]$, $a>0$ and $H(r)$ is the step function

$$H(r)=\begin{cases} 1, & r\geqslant 0, \\ 0, & r<0. \end{cases}$$
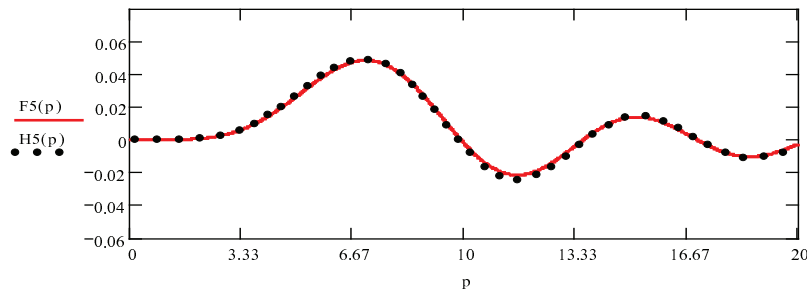
Figure 13: The exact transform, $F5(p)$ (solid line) and the approximate transform, $H5(p)$ (dotted-line) truncated at level $N=50$ and $M=2$ ($\nu=5$).
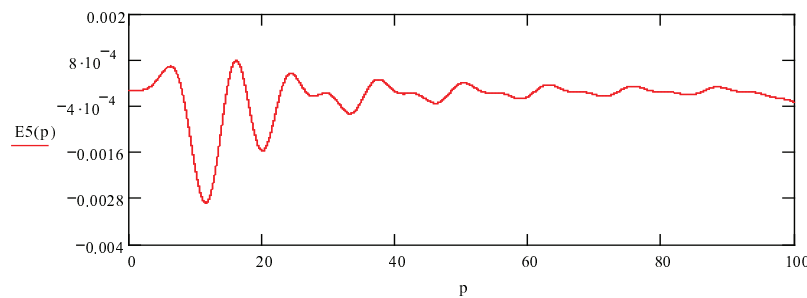
Figure 14: Error between exact transform, $F5(p)$ and approximated transform $H5(p)$ (without random noise) ($\nu=5$).
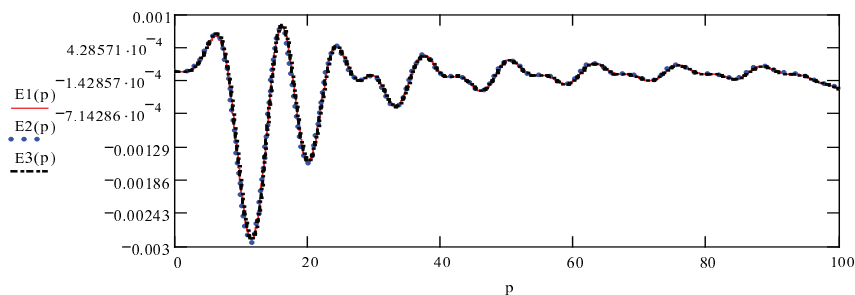
Figure 15: Errors between exact transform and approximated transform with different random perturbations ($\nu=5$).

Then,

$$F_\nu(p) = \frac{J_{\nu+1}(p)}{p}.$$

In [34], authors took $a=1$ and $\nu=4$ for numerical calculations. We take $a=1$, $\nu=1/10,5$ and observe that the errors are quite small as shown in Figs. 11 and 14 respectively. The corresponding errors $Ej(p)$ with different level of random noises are shown in Figs. 12 and 15 and Figs. 10 and 13 show the comparison between the exact transform and the approximate transform for $\nu=1/10,5$ respectively.
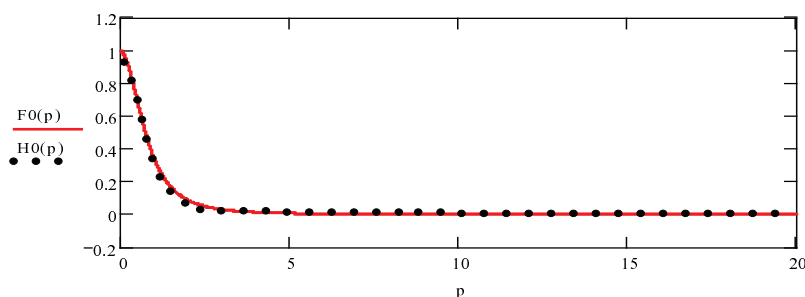
Figure 16: The exact transform, $F0(p)$ (solid line) and the approximate transform, $H0(p)$ (dotted-line) truncated at level $N=65$ and $M=2$.
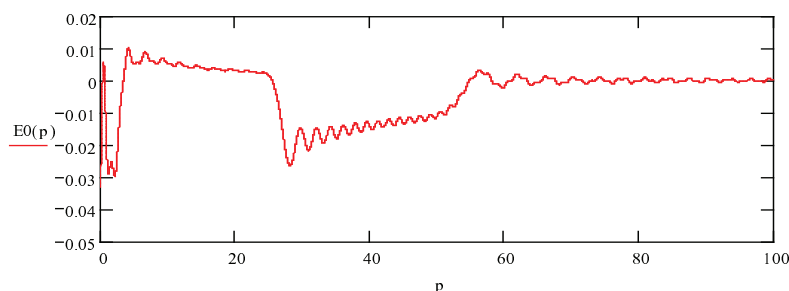
Figure 17: Error between exact transform, $S0(p)$ and approximated transform $H0(p)$ (without random noise).
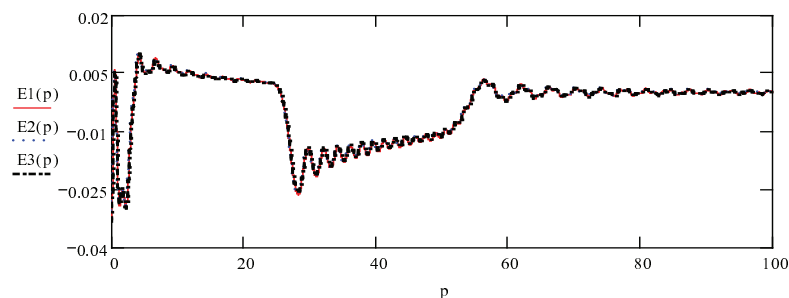
Figure 18: Errors between exact transform and approximated transform with different random perturbations.

Example 4.5. The following example was solved numerically by Knockaert [15]. For

$$f(r) = e^{-r}, \quad \text{its HT is } F_0(p) = \frac{1}{(1+p^2)^{3/2}}.$$

We solve the above problem by the proposed algorithm and observe that our method give result comparable to [15]. Note that $F_0(p)$ and $\hat{F}_0(p)$ are indicated by $F0(p)$ (solid line) and $H0(p)$ (dotted line) in Figs. 16 and 17 respectively. Figs. 17 and 18 depict the associated errors $Ej(p)$ for $j=0$ and $j=1,2,3$ respectively.

5 Application

As an application, we solve the heat equation in cylindrical coordinates inside an infinitely long cylinder of radius unity, by using the theory of Hankel transform developed in the preceding pages. We seek a function $u(r,t)$; where r is radius and t is time, (u does not depend on θ and t) satisfying the differential equation

$$D_r^2 u + \frac{1}{r} D_r u = D_t u \qquad (0 < r < 1, \ 0 < t < \infty) \tag{5.1}$$

and the following initial and boundary conditions:

(i) As $t \to 0^+, u(r,t) \to f(r) = \frac{2}{\pi} \left[\arccos(r) - r(1-r^2)^1/2 \right]$, $0 \le r \le 1$.

(ii) As $r \to 1^-, D_r u + H u \to 0$ for each fixed $t > 0$, where $H > 0$.

When u denotes the temperature within the cylinder, $H > 0$ means that heat is being radiated away from the surface of the cylinder.

Let $\Omega_{v,r}$ denotes the differential operator $D_r^2 + \frac{1}{r} D_r - \frac{v^2}{r^2}$. Then the differential equation (5.1) can be written as

$$\Omega_{0,r} u = \frac{\partial u}{\partial t}. \tag{5.2}$$

The Dini expansion associated with $f(r)$ is

$$B_0(r) + \sum_{m=1}^{\infty} b_m J_v(\lambda_m r), \qquad [\,48,\, \text{p.596}\,] \tag{5.3}$$

where λ_m, $m=1,2,3,\cdots$, are the positive rots (arranged in ascending order of magnitude) of the transcendental equation

$$z J_v'(z) + H J_v(z) = 0, \qquad v \ge -\frac{1}{2}, \tag{5.4}$$

b_m, $m=1,2,3,\cdots$, are given by

$$b_m = \frac{2\lambda_m^2 \displaystyle\int_0^1 r f(r) J_v(\lambda_m r) dr}{(\lambda_m^2 - v^2) J_v^2(\lambda_m) + J_v'^2(\lambda_m)} \tag{5.5}$$

and $B_0(r) = 0$ if $H + v > 0$, which is the case for the present problem as $v = 0$ and $H > 0$. The condition of validity of (5.3) are given in the following theorem [48, p. 601].

Theorem 5.1. *Let $f(r)$ be a function defined over the interval $(0,1)$, and let $\int_0^1 r^{1/2} f(r) dr$ exist and (if it is improper integral) let it be absolutely convergent. If $f(r)$ has limited total fluctuation in (a,b) where $0 \le a < b \le 1$ then the series (5.3) converges to the sum $\frac{1}{2}[f(r+0) + f(r-0)]$ at all points r such that $a + \Delta \le r \le b - \Delta$ where Δ is arbitrarily small; and the convergence is uniform if $f(r)$ is continuous in (a,b).*

Substituting Eqs. (3.1) and (5.5) into (5.3) and using the above theorem, we obtain the following inversion theorem for the finite Hankel transform.

Theorem 5.2 (Inversion). *Let $f(r)$ satisfies condition of Theorem 5.1, then*

$$f(r) = \lim_{N \to \infty} \sum_{m=1}^{N} \frac{2\lambda_m^2 \hat{F}_\nu(\lambda_m) J_\nu(\lambda_m r)}{(\lambda_m^2 - \nu^2) J_\nu^2(\lambda_m) + J_\nu'^2(\lambda_m)}. \tag{5.6}$$

From the well known formula

$$\Omega_{0,r} J_0(\lambda_m r) = -\lambda_m^2 J_0(\lambda_m r), \tag{5.7}$$

it follows from integration by parts that

$$\int_0^1 [\Omega_{0,r} f(r)] r J_0(\lambda_m r) dr = \int_0^1 f(r) r \Omega_{0,r} J_0(\lambda_m r) dr$$
$$= -\lambda_m^2 \int_0^1 f(r) r J_0(\lambda_m r) dr, \tag{5.8}$$

if we put some suitable condition on $f(r)$ such that the limit terms in integration by parts in (5.8) *vanish.*

Applying the finite Hankel transform operator to Eq. (5.2) and using (5.8), we obtain

$$-\lambda_m^2 U(\lambda_m, t) = \frac{\partial U(\lambda_m, t)}{\partial t},$$

where

$$U(\lambda_m, t) = \int_0^1 U(r, t) r J_0(\lambda_m r) dr,$$

so that

$$U(\lambda_m, t) = A(\lambda_m) e^{-\lambda_m^2 t}.$$

The initial condition determines the constant A. Thus

$$A(\lambda_m) = \hat{F}_0(\lambda_m) = \int_0^1 f(r) r J_0(\lambda_m r) dr.$$

Hence

$$U(\lambda_m, t) = \hat{F}_0(\lambda_m) e^{-\lambda_m^2 t}.$$

Therefore, by Inversion Theorem 5.2, we have

$$U(r, t) = \lim_{N \to \infty} \sum_{m=1}^{N} \frac{2\hat{F}_0(\lambda_m) e^{-\lambda_m^2 t} J_0(\lambda_m r)}{J_0^2(\lambda_m) + J_1^2(\lambda_m)}, \tag{5.9}$$

since $J_0'(r) = -J_1(r)$.
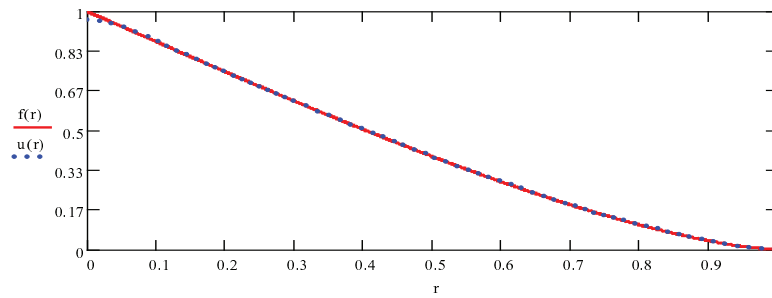
Figure 19: The initial condition function $f(r)$ (solid line) and $u(r)(=\lim_{t\to 0^+}u(r,t))$ (dotted line).
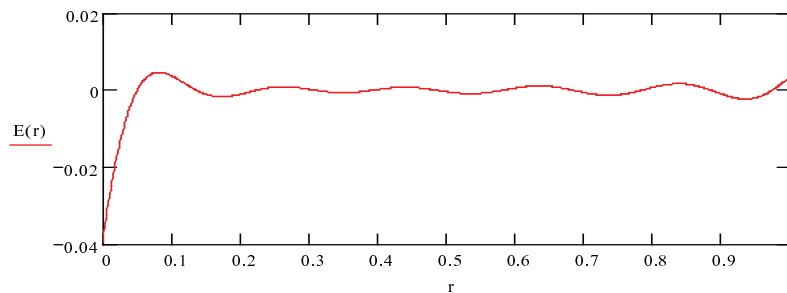
Figure 20: Error between $f(r)$ and $u(r)$.

We want to prove that $u(r,t)$, given by (5.9) is truly a solution of (5.1) that satisfies the given initial and boundary conditions. To achieve this, we need the following well known estimates:

$$F_0(\lambda_m) = \mathcal{O}(\lambda_m^{-\frac{3}{2}}) \qquad \text{as} \quad m\to\infty, \qquad [48, \text{p. 595}]$$

$$\lambda_m \sim \pi(m+\frac{1}{4}) \qquad \text{as} \quad m\to\infty,$$

$$J_0^2(\lambda_m) + J_1^2(\lambda_m) \sim \frac{2}{\pi\lambda_m} \quad \text{as} \quad m\to\infty.$$

Hence

$$F_0(\lambda_m)[J_0^2(\lambda_m) + J_1^2(\lambda_m)]^{-1} = \mathcal{O}(m^{-1/2}) \quad \text{as} \quad m\to\infty.$$

Using the above estimates, we see that the series (5.9) and the series obtained by applying $\Omega_{0,r}$ and D_t separately under the summation sign of (5.9) converges uniformly on $0<r<1$ and $t>0$. Hence by applying $\Omega_{0,r}-D_t$ and using the fact

$$\Omega_{0,r}[J_0(\lambda_m r)] = -\lambda_m^2 J_0(\lambda_m r),$$

we see that (5.9) satisfies the differential equation (5.1).
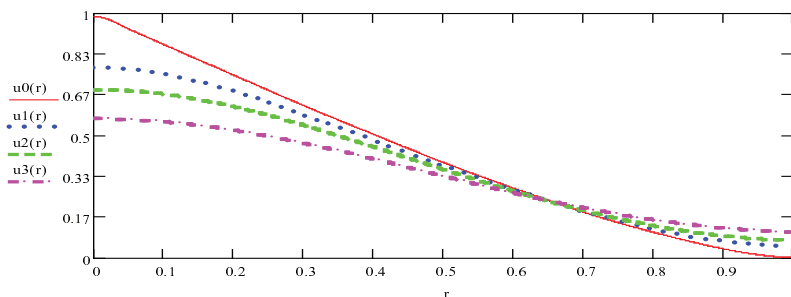
Figure 21: The various profiles of the solutions $u(r,t)$ at fixed times.
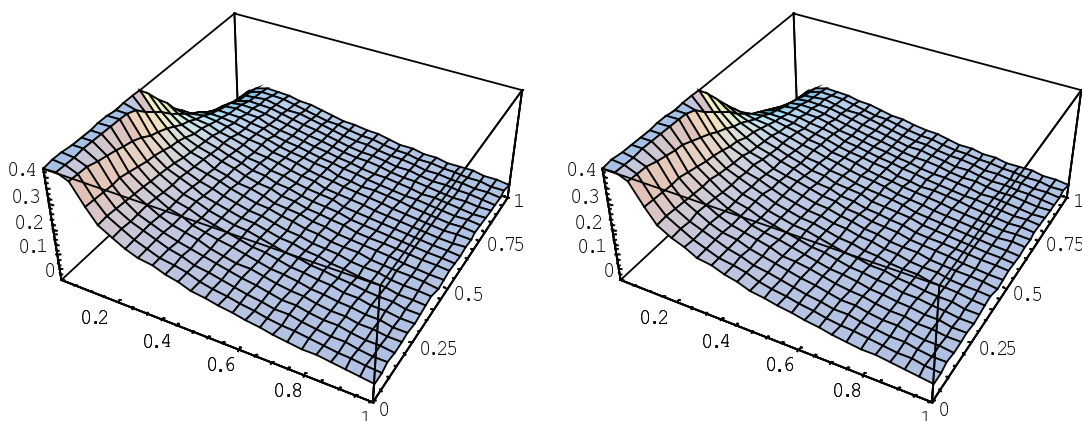
Figure 22: The solution $u(r,t)$ (left) and $u_a(r,t)$ (right) for $0<t<1$ and $0<r<1$.

Let us verify the boundary condition (ii), we have

$$\lim_{r \to 1^-} [D_r u + Hu]$$

$$= \lim_{r \to 1^{-1}} \left[\sum_{m=1}^{\infty} D_r \left\{ \frac{2\hat{F}_0(\lambda_m)e^{-\lambda_m^2 t} J_0(\lambda_m r)}{J_0^2(\lambda_m) + J_1^2(\lambda_m)} \right\} + H \sum_{m=1}^{\infty} \frac{2\hat{F}_0(\lambda_m)e^{-\lambda_m^2 t} J_0(\lambda_m r)}{J_0^2(\lambda_m) + J_1^2(\lambda_m)} \right]$$

and since the convergence is uniform, we can take the $\lim r \to 1^-$ inside the summation sign and arrive at the conclusion, since λ_m's are the roots of the equation

$$\lambda J_0'(\lambda) + H J_0(\lambda) = 0.$$

The initial condition (i) is already taken care of as we evaluated the constant A by using it. Through Figs. 19-22, we establish the accuracy of the propose method. All figures are drawn by truncating the series (5.9) at $N=10$. The presence of $e^{-\lambda_m^2 t}$ ensures that even ten terms give satisfactory solution for $t>0$. While evaluating the solution $u(r,t)$ from (5.9), we have evaluated $\hat{F}_0(\lambda_m)$ first from its analytical expression given by (4.4) and denote the solution thus obtained by $u(r,t)$ in Figs. 19-22 and then evaluating

Table 1: Error norm as function of ε in Example 4.1.

EXAMPLE 4.1	ERROR NORMS (DISCRETE l^2)			ERROR
ε	$N=10000$	$N=5000$	$N=1000$	NORMS(L^2)
0.000	0.00000005	0.00000003	0.00000001	0.00000046
0.001	0.00000955	0.00000675	0.00000296	0.00009609
0.002	0.00000677	0.00000576	0.00000257	0.00006790
0.005	0.00002572	0.00001969	0.00000879	0.00025728

Table 2: Error norm as function of ε in Example 4.2.

EXAMPLE 4.2	ERROR NORMS (DISCRETE l^2)			ERROR
ε	$N=10000$	$N=5000$	$N=1000$	NORMS(L^2)
0.000	0.00010522	0.00136662	0.00066664	0.00105925
0.001	0.00010561	0.00135265	0.00065982	0.00105815
0.002	0.00010671	0.00137143	0.00066898	0.00107677
0.005	0.00010790	0.00134560	0.00065637	0.00109293

Table 3: Error norm as function of ε in Example 4.3.

EXAMPLE 4.3	ERROR NORMS (DISCRETE l^2)			ERROR
ε	$N=10000$	$N=5000$	$N=1000$	NORMS(L^2)
0.000	0.00066952	0.00051330	0.00023021	0.00622474
0.001	0.00066813	0.00051254	0.00022987	0.00620880
0.002	0.00066986	0.00051298	0.00023005	0.00623324
0.005	0.00067195	0.00051507	0.00023100	0.00624634

$\hat{F}_0(\lambda_m)$ by using the proposed algorithm for evaluation of the finite Hankel transform as given by equation (3.8). This solution is denoted by $u_a(r,t)$ in the above mentioned figures.

Fig. 19, compares the given initial condition $f(r)$ with $u(r,t)$ as $t \to 0^+$ and Fig. 20 shows the error corresponding error $E(r) = u(r,0) - f(r)$. Fig. 21 depicts the various profiles of $u_i(r,t)$ at times $t = 0, 1/100, 1/50$ and $1/25$, the various profiles are denoted by u_0, u_1, u_2 and u_3. As the maximum possible error occurs in the neighbourhood of 0 and 0.001, we have restricted t in $(0,1]$ in Fig. 22 representing $u(r,t)$ and $u_a(r,t)$ respectively and note that they are in good agreement in the range.

6 Error analysis

The numerical stability property of the algorithm is illustrated in Tables 1-6 where the discrete l^2 norm as well as L^2 norm of the error is shown as a function of the amount of noise ε in the data function, for Examples 4.1-4.5 respectively (Example 4.4 has two Tables 4 and 5 for different order of HT for the same test function). We notice that in

Table 4: Error norm as function of ε in Example 4.4 ($\nu = 0.1$).

EXAMPLE 4.4 ($\nu = 1/10$)	ERROR NORMS (DISCRETE l^2)			ERROR
ε	$N = 10000$	$N = 5000$	$N = 1000$	NORMS(L^2)
0.000	0.00150236	0.00107089	0.00047783	0.01503314
0.001	0.00153680	0.00109493	0.00048854	0.01537775
0.002	0.00148723	0.00105750	0.00047179	0.01488198
0.005	0.00147326	0.00104688	0.00046706	0.01474207

Table 5: Error norm as function of ε in Example 4.4 ($\nu = 5$).

EXAMPLE 4.4 ($\nu = 5$)	ERROR NORMS (DISCRETE l^2)			ERROR
ε	$N = 10000$	$N = 5000$	$N = 1000$	NORMS(L^2)
0.000	0.00060155	0.00722909	0.00335988	0.00573836
0.001	0.00059574	0.00723622	0.00336320	0.00567961
0.002	0.00060788	0.00721697	0.00335424	0.00580418
0.005	0.00059563	0.00719988	0.00334632	0.00573836

Table 6: Error norm as function of ε in Example 4.5.

EXAMPLE 4.5	ERROR NORMS (DISCRETE l^2)			ERROR
ε	$N = 10000$	$N = 5000$	$N = 1000$	NORMS(L^2)
0.000	0.00891836	0.00630522	0.00282352	0.08897511
0.001	0.00892978	0.00631329	0.00282715	0.08908933
0.002	0.00883437	0.00624580	0.00279698	0.08813880
0.005	0.00878099	0.00620796	0.00278019	0.08760884

all the cases, the numerical stability of the proposed algorithm is confirmed. Moreover, in the ϵ range 0.000 to 0.005 the discrete error norms are barely sensitive to changes in $h = 1/N$ in Examples 4.1, 4.3, 4.4 ($\nu = 1/10$) and 4.5 and only slightly more sensitive to changes in h in Examples 4.2 and 4.4 ($\nu = 5$).

7   Summary and conclusions

A new method based on the Chebyshev wavelets for the numerical evaluation of HT is proposed and analyzed. As the basis functions used to construct the Chebyshev wavelets are orthogonal and have compact supports, it makes them more useful and simple in actual computations compared to the algorithm based on Chebyshev polynomials [46]. Also, since the number of mother wavelet's components is restricted to one, they do not lead to the growth of complexity of calculations. Our choice of wavelets make it more attractive in their application in the applied physical problems as they eliminate the problems connected with the Gibbs phenomenon taking place in [32, 34]. The error associated with Filon quadrature philosophy [6], [21, 21] is appreciable for small $p < 1$

compared to our algorithm.

The stability with respect to the data is restored and excellent accuracy is obtained even for small sample interval and high noise levels in the data. Several test cases are investigated by varying the number of sampling points N and amount of noise ε in the data. We notice that in all the cases, the numerical accuracy and stability of the proposed algorithm is confirmed.

Acknowledgment

References

[1] J.W. Goodman, Introduction to Fourier Optics. McGraw-Hill, New York, 1968.
[2] H.-Y. Fan, Hankel transform as a transform between two entangled state representations, Phys. Lett. A., 313 (2003) 343-350.
[3] I.N. Sneddon, The use of Integral Transforms. McGraw-Hill, 1972.
[4] V.S. Kulkarni, K.C. Deshmukh, An inverse quasi-static steady-state in a thick circular plate, J. Frank. Inst. 345 (1) (2008) 29-38.
[5] V. Magni, G. Cerullo, De Silvestri, High-accuracy fast Hankel transform for optical beam propagation, J. Opt. Soc. Am. A., 12 (1992) 2031-2033.
[6] R. Barakat, E. Parshall, B.H. Sandler, Zero-order Hankel transform algorithms based on Filon quadrature philosophy for diffraction optics and beam propagation, J. Opt. Soc. Am. A., 15 (1998) 652-659.
[7] N.T. Eldabe, M. El-Shahed , M. Shawkey, An extension of the finite Hankel transform, Appl. Math. Comput., 151 (2004) 713-717.
[8] D. Patella, Gravity interpretation using the Hankel transform, Geophysical Prospecting, 28 (1980) 744-749.
[9] D.R Mook, An algorithm for numerical evaluation of Hankel and Abel transform, IEEE Trans. Acoust. Speech Signal Process., ASSP-31 (1983) 979-985.
[10] E.C. Cavanagh, B.D. Cook, Numerical evaluation of Hankel Transform via Gaussian-Laguerre polynomial expressions, IEEE Trans. Acoust. Speech Signal Process., ASSP-27 (1979) 361-366.
[11] E.V. Hansen, Fast Hankel transform algorithms, IEEE Trans. Acoust. Speech Signal Process., ASSP-33 (1985) 666-671.
[12] E.V. Hansen, Correction to Fast Hankel transform algorithms, IEEE Trans. Acoust. Speech Signal Process., ASSP-34 (1986) 623-624.
[13] S.M. Candel, Dual algorithms for fast calculation of the Fourier Bessel transform, IEEE Trans. Acoust. Speech Signal Process., ASSP-29 (1981) 963-972.
[14] B.W. Suter, Fast nth order Hankel transform algorithm, IEEE Trans. Signal Process., 39 (1991) 532-536.
[15] L. Knockaert, Fast Hankel transform by fast sine and cosine transform: the Mellin connection, IEEE Trans. Signal Process., 48 (2000) 1695-1701.
[16] W.E. Higgins, D.C. Munson, A Hankel transform approach to tomographic image reconstruction, IEEE Trans. Med. Imag., 7 (1988) 59-72.

[17] O.P. Singh, J.N. Pandey, The Fourier-Bessel series representation of the pseudo differential operator $(-x^{-1}D)^\nu$, Proc. Amer. Math. Soc., 115 (4) (1992) 969-976.

[18] O.P. Singh, On pseudo-differential operator $(-x^{-1}D)^\nu$, J. Math. Anal. Appl., 191 (1995) 450-459.

[19] A.E. Siegman, Quasi Fast Hankel Transform, J. Optics. Lett., 1 (1977) 13-15.

[20] J.A. Ferrari, Fast Hankel transform of order zero, J. Opt. Soc. Am. A., 12 (1995) 1812-1813 .

[21] R. Barakat, E. Parshall, Numerical evaluation of the zero-order Hankel transform using Filon quadrature philosophy, Appl. Math. Lett., 9(5) (1996) 21-26.

[22] R. Barakat, B. H. Sandler, Evaluation of first-order Hankel transforms using Filon quadrature philosophy, Appl. Math. Lett., 11(1) (1998) 127-131.

[23] Li Yu, M. Huang, M. Chen, W. Huang, Z. Zhu, Quasi-discrete Hankel transform, Opt. Lett., 23 (1998) 409- 411.

[24] J. Markham, J.A. Conchello, Numerical evaluation of Hankel transform for oscillating function, J. Opt. Soc. Am. A., 20 (2003) 621-630.

[25] P. K. Murphy, N.C. Gallagher, Fast algorithm for computation of zero-order Hankel transform, J. Opt. Soc. Am., 73 (2003) 1130-1137.

[26] A.V. Oppenheim, G.V. Frish, D.R. Martinez, An algorithm for numerical evaluation of Hankel transform, Proc. IEEE., 66 (1980) 264-265.

[27] A.V. Oppenheim, G.V. Frish, D.R. Martinez, Component of Hankel transform using projections, J. Acoust. Soc. Am., 68 (1980) 523-529.

[28] W.E. Higgins, D.C. Munsons, Jr., An algorithm for computing general integer order Hankel transforms, IEEE Trans. Acoust. Speech Signal Process., ASSP-35 (1987) 86-97.

[29] J.A. Ferrari, D. Peciante, A. Durba, Fast Hankel transform of nth order, J. Opt. Soc. Am. A., 16 (1999) 2581-2582.

[30] A.Agnesi, G.C. Reali, G. Patrini, A. Tomaselli, Numerical evaluation of the Hankel transform: remarks, J. Opt. Soc. Am. A., 10 (1993) 1872-1874.

[31] B.W. Suter , R.A. Hedges, Understanding fast Hankel transform, J. Opt. Soc. Am. A., 18 (2001) 717-720.

[32] E.B. Postnikov, About calculation of the Hankel transform using preliminary wavelet transform, J. Applied Math., 6 (2003) 319-325.

[33] R. Piessens, M. Branders, Modified Clenshaw-Curtis method for the computation of Bessel function integrals, BIT Numerical Mathematics, 23 (1983) 370-381.

[34] M. Guizar-Sicairos, J. C. Gutierrez-Vega, Computation of quasi-discrete Hankel transforms of integer order for propagating optical wave fields, J. Opt. Soc. Am. A., 21(1) (2004) 53.

[35] V.K. Singh, O.P. Singh, R.K. Pandey, Numerical evaluation of Hankel transform by using linear Legendre multi-wavelets, Compu. Phys. Commun. 179 (2008) 424-429.

[36] R.K. Pandey, V.K. Singh, O.P. Singh, , An improved method for computing Hankel transform, J. Franklin Inst.. (2008) (Accepted) doi: 10.1016/j.jfranklin.2008.07.002

[37] A. Haar, Zur theorie der orthogonalen funktionensysteme, Math. Ann., 69 (1910) 331-371.

[38] I. Daubechies, Orthonormal bases of compactly supported wavelets, Commun. Pure Appl. Math., 41 (1988) 909-996.

[39] I. Daubechies, Ten Lectures on Wavelets, CBMS-NSF, 1992.

[40] S. Mallat, Multiresolution approximation and wavelet orthonormal bases of $L^2(R)$, Trans. Amer. Math. Soc., 315 (1989) 69-87.

[41] S. Mallat, A theory for Multiresolution Signal decomposition: The wavelet representation, IEE Trans. Pattern Recogn. Mach. Intell., 11 (7) (1989) 674.

[42] R. M. Young, An Introduction to Nonharmonic Fourier Series, Academic Press, New York,

1980.

[43] E. Babolian, F. Fattahzadeh, Numerical solution of differential equations by using Chebyshev wavelet operational matrix of integration, Appl. Math. Comput., 188 (2007) 417-426.

[44] A.Erdelyi (Ed.), Tables of Integral Transforms, McGraw-Hill, New York, 1954.

[45] M. Abramowitz, I. A. Stegun, Handbook of Mathematical Functions, With Formulas, Graphs, and Mathematical Tables, Dover Publications, Inc., New York, 1965.

[46] R. Piessens, Computing integral transforms and solving integral equations using Chebyshev polynomial approximations, J. Comput. Appl. Math. , 121 (2000) 113-124.

[47] S. M. Candel, An algorithm for the Fourier Bessel transform, Comput. Phys. Commun., 23 (1981) 343.

[48] G. N. Watson, Theory of Bessel functions, 2nd ed., Cambridge University Press, 1958.